Enhancing the Robustness of the Wireless Power Transfer System to Uncertain Parameter Variations Using an Interval-Based Uncertain Optimization Method

Authors:

Yanting Luo, Yongmin Yang, Xisen Wen, Ming Cheng

Abstract:

Uncertainty commonly exists in the wireless power transfer (WPT) systems for moving objects. To enhance the robustness of the WPT system to uncertain parameter variations, a modified WPT system structure and an interval-based uncertain optimization method are proposed in this paper. The modified WPT system, which includes two Q-type impedance matching networks, can switch between two different operating modes. The interval-based uncertain optimization method is used to improve the robustness of the modified WPT system: First, two interval-based objective functions (mean function and variance function) are defined to evaluate the average performance and the robustness of the system. A double-objective uncertain optimization model for the modified WPT system is built. Second, a bi-level nested optimization algorithm is proposed to find the Pareto optimal solutions of the proposed optimization model. The Pareto fronts are provided to illustrate the tradeoff between the two objectives, and the robust solutions are obtained. Experiments were carried out to verify the theoretical method. The results demonstrated that using the proposed method, the modified WPT system can achieve good robustness when the coupling coefficient, the operating frequency, the load resistance or the load reactance varies over a wide range.

Enhancing the Robustness of the Wireless Power Transfer System to Uncertain Parameter Variations Using an Interval-Based Uncertain Optimization Method

Yanting Luo *, Yongmin Yang, Xisen Wen and Ming Cheng

Science and Technology on Integrated Logistics Support Laboratory, National University of Defense Technology, Changsha 410073, China; yangyongmin@163.com (Y.Y.); wenxs@vip.sina.com (X.W.); chengming12@nudt.edu.cn (M.C.)
* Correspondence: luoyanting0717@126.com

Abstract: Uncertainty commonly exists in the wireless power transfer (WPT) systems for moving objects. To enhance the robustness of the WPT system to uncertain parameter variations, a modified WPT system structure and an interval-based uncertain optimization method are proposed in this paper. The modified WPT system, which includes two Q-type impedance matching networks, can switch between two different operating modes. The interval-based uncertain optimization method is used to improve the robustness of the modified WPT system: First, two interval-based objective functions (mean function and variance function) are defined to evaluate the average performance and the robustness of the system. A double-objective uncertain optimization model for the modified WPT system is built. Second, a bi-level nested optimization algorithm is proposed to find the Pareto optimal solutions of the proposed optimization model. The Pareto fronts are provided to illustrate the tradeoff between the two objectives, and the robust solutions are obtained. Experiments were carried out to verify the theoretical method. The results demonstrated that using the proposed method, the modified WPT system can achieve good robustness when the coupling coefficient, the operating frequency, the load resistance or the load reactance varies over a wide range.

Keywords: wireless power transfer; uncertain parameter variations; interval-based uncertain optimization; tradeoff decision; robustness

---

1. Introduction

In recent years, wireless power transfer (WPT) for moving objects using coupled magnetic resonance (CMR) has become a hot research topic, such as WPT for portable electronic devices and moving electric vehicles [1–3]. Unlike WPT systems for stationary objects, there are many uncertain parameters in the WPT systems for moving objects. For example, because users prefer to move the receiver freely, the distance between the transmitter and receiver coils is uncertain [4,5]. In addition, the magnetic field of the dynamic charging system is prone to interact with the objects around it, such as metal materials, and electromagnetic devices, etc. These external uncertain factors will change the impedance parameters of the circuit and make the resonance frequency of the system uncertain [6,7]. Moreover, the load impedance of the WPT system will be influenced by many uncertain factors, including environmental change, and load switching, etc. [8–10] The load impedance variations will also bring uncertainty to the WPT system.

As we know, the efficiency and output power of the WPT system will be maximized if the system satisfies the optimal impedance matching condition [11]. However, the uncertain parameter variations

will change the impedance characteristics of the transmitter and/or the receiver, and hence break the impedance matching status of the overall WPT system. As a result, the system efficiency and the power received by the load will decrease rapidly.

Many works [12–19] have been done to improve the performance of the WPT system with uncertain parameters. In [12], an adaptive frequency-tracking technique is proposed to address coil distance and orientation variations. Through the method, the WPT system can maintain nearly constant efficiency when the user moves the receiver within a short range.

Because the frequency tracking technique can only be used when the coils are strongly coupled [13,14], impedance matching network methods [15,16] using energy-storage components are proposed. In [15], an impedance matching network was inserted into the transmitter-circuit so that the impedance of the transmitter can be dynamically matched to the source impedance. This method allows the WPT system to be robust toward coil misalignments and load impedance variations.

An automatic load resistance transformation method is proposed in [18]. A receiver-side switching converter was used to transform the load resistance into an optimum resistance, based on the measured coil distance and load current information. In this way, the WPT system can maintain high efficiency under the variations of coil distance and load current. Aiming at improving the robustness for moving robot wireless power supplies, it proposed in [19] that a H_∞ control method for the WPT system with multiple uncertain parameters. Using this control method, the WPT system can achieve 70% mutual inductance variation and 50% load variation tolerance.

Although these methods can improve the performance of the WPT system with uncertain parameter variations, there still exist some drawbacks: (1) To deal with uncertain parameter variations, an active compensation system (like frequency tracking system, automatic impedance matching system, and H_∞ control system, etc.) is needed [12–19]. However, introducing the active compensation system will obviously increase the size, control difficulty, and energy losses of the overall WPT system. In some situations, the respond speed of the active compensation system cannot catch up with the changing speed of the uncertain parameters [20]; (2) To implement active control, real-time information of the uncertain parameters is needed [21–23]. However, because the uncertain parameters in the WPT system often change rapidly and randomly, it is very difficult and expensive to obtain the real-time information for them in engineering practice. Even a small measurement error can result in a large deviation of the system response. Therefore, there is a need to explore more efficient ways to address uncertain parameter variations.

In this paper, a modified WPT system structure and an interval-based uncertain optimization method are proposed to address uncertain parameters variations. Based on the method, an interval is used to model the uncertainty of a parameter in the WPT system. Thus, the WPT system can be analyzed and optimized based on the variation bounds of the uncertain parameters. There is no need to measure the real-time information of the uncertain parameters. Using the proposed method, the WPT system can achieve good robustness to uncertain parameter variations. Compared with previous methods [12–19], the proposed method only uses passive compensation networks (Q-type impedance matching networks). The structure and control difficulty of the overall WPT system can be reduced. In addition, the proposed method is not affected by the changing speed of the uncertain parameters.

The rest of the paper is organized as follows: Section 2 investigates the effects of uncertain parameter variations on the WPT system performance; Section 3 proposes a modified WPT system structure and an interval-based uncertain optimization method to address uncertain parameter variations; Section 4 shows the experimental results, and, finally, conclusions are provided in Section 5.

2. Modeling and Analysis of the WPT System with Uncertainty

2.1. Uncertain Parameters in the WPT System

Figure 1 shows the structure of a WPT system using CMR. A power source is used to supply high-frequency power to the transmitter coil. The power is transmitted from the transmitter coil to the

receiver coil through magnetic coupling. A load is used to consume the power received by the receiver coil. Two tuning and impedance matching circuits are used to compensate the reactive power in the WPT system.
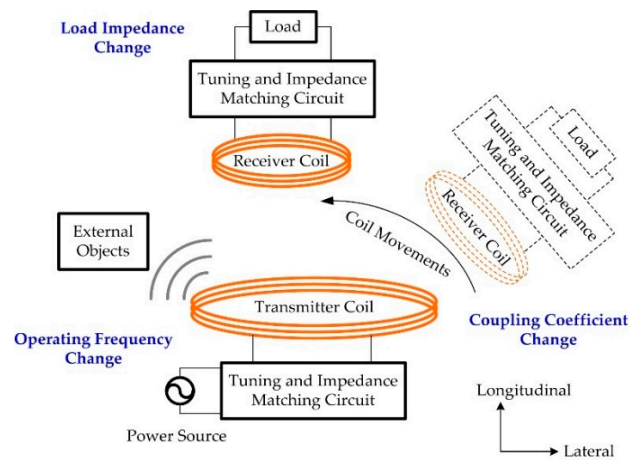

Figure 1. Structure of a WPT system using CMR.

In this paper, the following uncertain parameters are mainly investigated:

First, the coupling coefficient *k* between the transmitter and receiver coils is one uncertain parameter. As shown in Figure 1, the receiver coil movement may lead to lateral, longitudinal, and angular displacements between the coils. The influence of the coil displacements on the WPT system is reflected in the change of the coupling coefficient.

Second, the operating frequency *f* is another uncertain parameter in the WPT system. Some uncertain factors, such as external objects, etc., will change the inherent frequency of the WPT system. To achieve resonance, the operating frequency should dynamically change according to the inherent frequency variation of the circuit.

Third, the load impedance Z_L is another uncertain parameter in the WPT system. In many practical applications, the load is not a pure resistance but a complex impedance. The load resistance R_L and the load reactance X_L will change dynamically with temperature rise, load switching, and many other uncertain factors.

2.2. Modeling of the WPT System

To analyze the effects of uncertain parameters on the WPT system performance, a cascade two-port network model of the WPT system is proposed. As shown in Figure 2, the WPT system is divided into five parts: The power source, the two-port network I, the two-port network II, the two-port network III, and the load. The port voltages and currents and the transmission parameters of the two-port networks are used to analyze the WPT system.
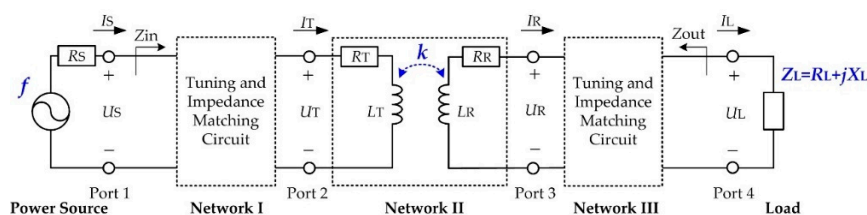

Figure 2. Cascade two-port network model of the WPT system.

2.2.1. Transmitter Coil and Receiver Coil

The two-port network II includes the transmitter and receiver coils. The input and output characteristics of the two-port network II can be described as:

$$\begin{bmatrix} U_T \\ I_T \end{bmatrix} = \begin{bmatrix} A_{\mathrm{II}} & B_{\mathrm{II}} \\ C_{\mathrm{II}} & D_{\mathrm{II}} \end{bmatrix} \begin{bmatrix} U_R \\ I_R \end{bmatrix} \tag{1}$$

where U_T and I_T are the voltage and current at Port 2, U_R and I_R are the voltage and current at Port 3. A_{II}, B_{II}, C_{II}, D_{II} are the transmission parameters the two-port network II, which can be calculated as:

$$\begin{cases} A_{\mathrm{II}} = \frac{R_T + j\omega L_T}{j\omega k\sqrt{L_T L_R}}, B_{\mathrm{II}} = \frac{(R_R + j\omega L_R)(R_T + j\omega L_T) + \omega^2 k^2 L_T L_R}{j\omega k\sqrt{L_T L_R}} \\ C_{\mathrm{II}} = \frac{1}{j\omega k\sqrt{L_T L_R}}, D_{\mathrm{II}} = \frac{R_R + j\omega L_R}{j\omega k\sqrt{L_T L_R}} \end{cases} \tag{2}$$

where L_T and L_R are the inductances of the transmitter coil and the receiver coil respectively, R_T and R_R are the resistances of the transmitter coil and the receiver coil respectively, k is the coupling coefficient between the coils, and ω is the angular operating frequency.
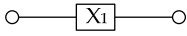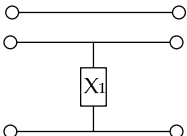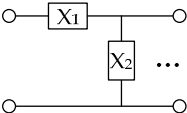
2.2.2. Tuning and Impedance Matching Circuits

The two-port network I includes the tuning and impedance matching circuit at the transmitter-side. The two-port network III includes the tuning and impedance matching circuit at the receiver-side. The input and output characteristics of each can be described as:

$$\begin{bmatrix} U_S \\ I_S \end{bmatrix} = \begin{bmatrix} A_{\mathrm{I}} & B_{\mathrm{I}} \\ C_{\mathrm{I}} & D_{\mathrm{I}} \end{bmatrix} \begin{bmatrix} U_T \\ I_T \end{bmatrix} \& \begin{bmatrix} U_R \\ I_R \end{bmatrix} = \begin{bmatrix} A_{\mathrm{III}} & B_{\mathrm{III}} \\ C_{\mathrm{III}} & D_{\mathrm{III}} \end{bmatrix} \begin{bmatrix} U_L \\ I_L \end{bmatrix} \tag{3}$$

where U_S and I_S are the voltage and current at Port 1, U_L and I_L are the voltage and current at Port 4. A_{I}, B_{I}, C_{I}, D_{I} and A_{III}, B_{III}, C_{III}, D_{III} are the transmission parameters of the two-port network I and the two-port network III, respectively.

There are many types of tuning and impedance matching circuits for the WPT system [24,25]. Table 1 shows the topologies and transmission parameters of some commonly used circuits, in which X_n $(n = 1, 2, \cdots)$ is a reactive power compensation unit, like a capacitor or an inductor.

Table 1. Some commonly used tuning and impedance matching circuits.

Type	Topology	Transmission Parameters
Series		$\mathbf{T}_S = \begin{bmatrix} 1 & jX_1 \\ 0 & 1 \end{bmatrix}$
Parallel		$\mathbf{T}_P = \begin{bmatrix} 1 & 0 \\ \frac{1}{jX_1} & 1 \end{bmatrix}$
Combination		$\mathbf{T}_C = \mathbf{T}_S^1 \times \mathbf{T}_P^2 \times \cdots$

2.2.3. Overall WPT System

The overall WPT system is the cascade system of the power source, the two-port network I, the two-port network II, the two-port network III, and the load. The input and output characteristics of the overall WPT system can be described as:

$$\begin{bmatrix} U_S \\ I_S \end{bmatrix} = \begin{bmatrix} A_I & B_I \\ C_I & D_I \end{bmatrix} \begin{bmatrix} A_{II} & B_{II} \\ C_{II} & D_{II} \end{bmatrix} \begin{bmatrix} A_{III} & B_{III} \\ C_{III} & D_{III} \end{bmatrix} \begin{bmatrix} U_L \\ I_L \end{bmatrix} = \begin{bmatrix} A & B \\ C & D \end{bmatrix} \begin{bmatrix} U_L \\ I_L \end{bmatrix} \tag{4}$$

where A, B, C, D represent the transmission parameters of the overall WPT system, which can be calculated as:

$$\begin{cases} A = A_{III}(A_I A_{II} + B_I C_{II}) + C_{III}(A_I B_{II} + B_I D_{II}), & B = B_{III}(A_I A_{II} + B_I C_{II}) + D(A_I B_{II} + B_I D_{II}) \\ C = A_{III}(A_{II} C_I + C_{II} D_I) + C_{III}(B_{II} C_I + D_I D_{II}), & D = B_{III}(A_{II} C_I + C_{II} D_I) + D_{III}(B_{II} C_I + D_I D_{II}) \end{cases} \tag{5}$$

Based on Equation (4), the input and output impedances of the WPT system can be calculated.

$$Z_{in} = \frac{U_S}{I_S} = \frac{AZ_L + B}{CZ_L + D} \ \& \ Z_{out} = -\frac{U_L}{I_L} = \frac{DR_S + B}{CR_S + A} \tag{6}$$

where R_S is the source internal resistance. Z_L is the load impedance, which usually includes a resistance part R_L, and a reactance part X_L.

A matching factor Z is defined to evaluate the impedance matching status of the system.

$$Z = |Z_{in} - R_S^*| + |Z_{out} - Z_L^*| \tag{7}$$

where R_S^* and Z_L^* are the conjugate values of R_S and Z_L. If $Z = 0$, the WPT system can achieve dual-side conjugate impedance matching.

The source output power can be calculated as:

$$P_S = |I_S|^2 R_{in} = \left| \frac{V_0}{R_S + Z_{in}} \right|^2 R_{in} \tag{8}$$

where V_0 is the source voltage, R_{in} is the real part of the input impedance Z_{in}.

The power delivered to the load can be calculated as:

$$P_L = |I_L|^2 R_L = \left| \frac{(A - CZ_{in})V_0}{(AD - BC)(R_S + Z_{in})} \right|^2 R_L \tag{9}$$

In previous studies [26–28], the transmission efficiency η_T was defined as the ratio of the load power to the source output power.

$$\eta_T = \frac{P_L}{P_S} = \left| \frac{A - CZ_{in}}{AD - BC} \right|^2 \frac{R_L}{R_{in}} \tag{10}$$

However, the transmission efficiency η_T cannot reflect the load power level. Because the source output power P_S is uncertain, the load power P_L can be low even if the transmission efficiency η_T is high.

To solve this problem, the system efficiency η_S is defined in this paper. It refers to the ratio of the load power to the maximum source output power.

$$\eta_S = \frac{P_L}{P_{S-\max}} \tag{11}$$

where $P_{S-\max}$ is the maximum source output power, which can be calculated as:

$$P_{S-\max} = P_S|_{Z_{in}=R_S} = \frac{V_0^2}{4R_S} \tag{12}$$

By substituting Equations (6), (9), and (12) into Equation (11), the system efficiency η_S can be obtained.

$$\eta_S = 4R_S R_L \left| \frac{1}{(A + CR_S)(R_L + jX_L) + B + DR_S} \right|^2 \tag{13}$$

The system efficiency η_S can reflect the utilization ratio of the maximum extractable power from the WPT system. If the system efficiency η_S is high, both the transmission efficiency η_T and the load power P_L will be high.

2.3. Analysis of the Uncertain Parameters

In this paper, the system efficiency is used to evaluate the performance of the WPT system. The effects of uncertain parameters on the system efficiency are analyzed using numerical simulations. The series–series (SS) compensated WPT system (which is one of the most commonly used structures [29–31]) is chosen to carry out the analysis. The simulation parameters are shown in Table 2. Based on Equations (7) and (13), the matching factor and the system efficiency can be calculated.

Table 2. Simulation parameters of the SS compensated WPT system.

Certain Parameter	Value
Source resistance R_S	50 Ω
Coil resistances R_T, R_R	1 Ω
Coil inductances L_T, L_R	30 µH
Series Capacitors C_T, C_R	211 pF
Uncertain Parameter	**Variation Range**
Coupling coefficient k	$0.1 \sim 0.6$
Operating frequency f	$1.5 \sim 2.5$ MHz
Load resistance R_L	$100 \sim 1500$ Ω
Load reactance X_L	$-800 \sim 800$ Ω

To simplify the analysis, only one uncertain parameter is varied at a time. When the coupling coefficient k, the operating frequency f, the load resistance R_L or the load reactance X_L varies, the calculated system efficiencies (blue solid line) and matching factors (red dashed line) are shown in Figure 3a–d, respectively. It can be observed that the system efficiency increases at first and then decreases with the increase of the uncertain parameter. On the contrary, the matching factor decreases at first and then increases with the increase of the uncertain parameter. The highest system efficiency can only be achieved when $Z = 0$.

The simulation results show that: (1) The system efficiency of the SS compensated WPT system is very sensitive to uncertain parameter variations; (2) the system efficiency can be maximized only when the WPT system achieves dual-side conjugate impedance matching ($Z = 0$).
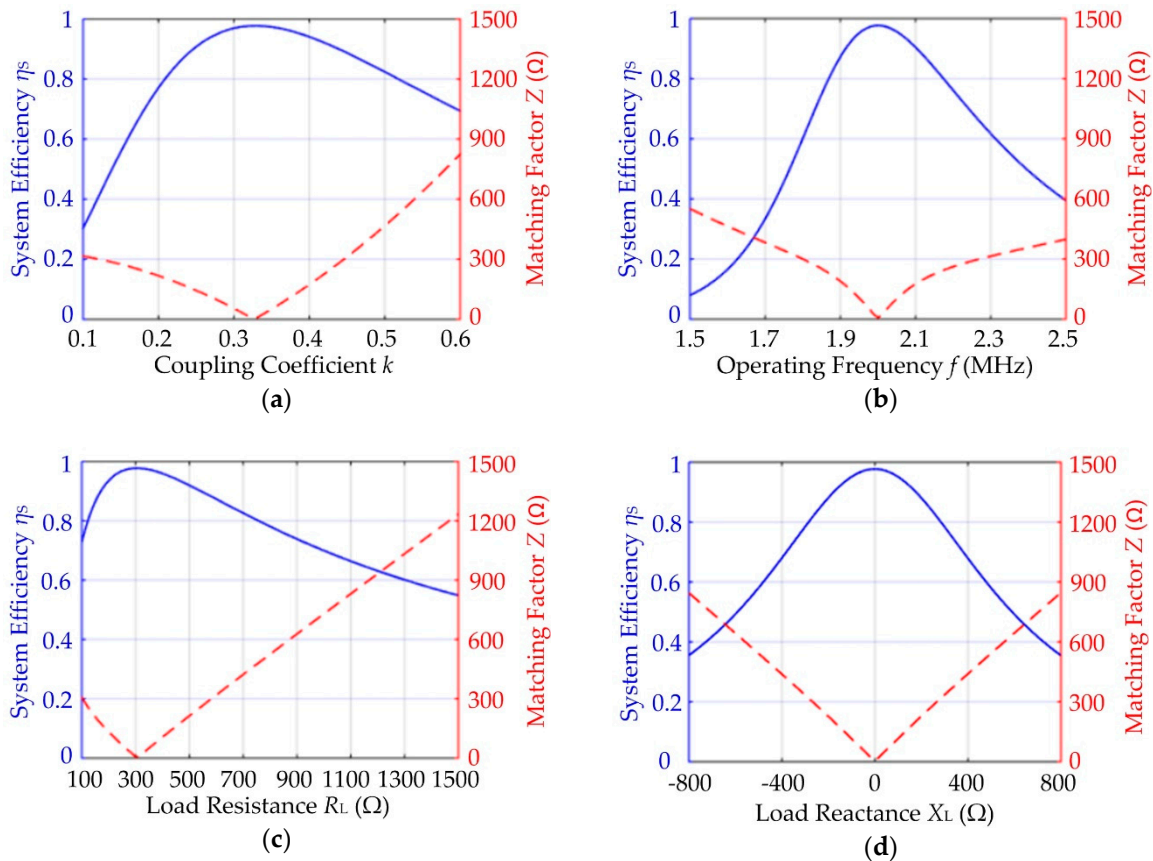
Figure 3. System efficiencies (blue solid line) and matching factors (red dashed line) of the SS compensated WPT system: (**a**) the coupling coefficient k varies from 0.1 to 0.6; (**b**) the operating frequency f varies from 1.5 to 2.5 MHz; (**c**) the load resistance R_L varies from 100 to 1500 Ω; (**d**) the load reactance X_L varies from -800 to 800 Ω. (The initial values of the uncertain parameters are: $k = 0.33$, $f = 2$ MHz, $R_L = 300$ Ω, and $X_L = 0$ Ω).

3. Interval-Based Uncertain Optimization Method for the WPT System

3.1. A Modified WPT System Structure

To enhance the robustness of the WPT system to uncertain parameter variations, a modified WPT system structure is proposed. As shown in Figure 4, it consists of a power source, a transmitter coil, a receiver coil, a complex load, and two Q-type impedance matching networks.
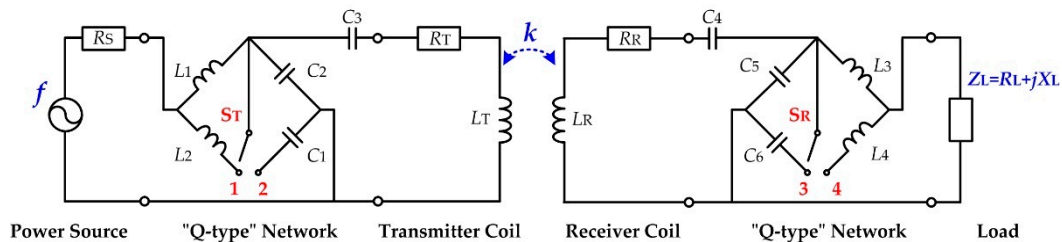

Figure 4. Structure of the modified WPT system.

The Q-type impedance matching network at the transmitter-side includes two compensation inductors (L_1, L_2) and three compensation capacitors (C_1, C_2, C_3). Similarly, the Q-type impedance matching network at the receiver-side includes two compensation inductors (L_3, L_4) and three compensation capacitors (C_4, C_5, C_6). There are two single pole double throw switches (S$_T$ and S$_R$) in

the Q-type impedance matching networks. As shown in Figure 4, S_T can switch between point 1 and point 2, and S_R can switch between point 3 and point 4.

The modified WPT system has two operating modes. The single-pole double-throw switches are used to switch the operating mode of the system. Table 3 shows the states of the switches (S_T and S_R) and the transmission parameters of the Q-type impedance matching networks at different operating modes.

Table 3. Two operating modes of the modified WPT system.

Switch States	Transmission Parameters of the Q-type Network at Transmitter-Side	Transmission Parameters of the Q-type Network at Receiver-Side
Mode 1: $S_T \to$ point 1 $S_R \to$ point 3	$\begin{cases} A_I = -\frac{\omega^2 C_2 L_1 L_2}{L_1+L_2} + 1 \\ B_I = j(\frac{\omega^2 C_2 L_1 L_2}{L_1+L_2} - 1)(\frac{C_2+C_3}{\omega C_2 C_3}) + \frac{j}{\omega C_2} \\ C_I = j\omega C_2 \\ D_I = \frac{C_2}{C_3} + 1 \end{cases}$	$\begin{cases} A_{III} = \frac{C_5+C_6}{C_4} + 1 \\ B_{III} = j(\omega^2(C_5+C_6)L_3 - 1)(\frac{C_4+C_5+C_6}{\omega C_4(C_5+C_6)}) + \frac{j}{\omega(C_5+C_6)} \\ C_{III} = j\omega(C_5+C_6) \\ D_{III} = -\omega^2(C_5+C_6)L_3 + 1 \end{cases}$
Mode 2: $S_T \to$ point 2 $S_R \to$ point 4	$\begin{cases} A_I = -\omega^2(C_1+C_2)L_1 + 1 \\ B_I = j(\omega^2(C_1+C_2)L_1 - 1)(\frac{C_1+C_2+C_3}{\omega(C_1+C_2)C_3}) + \frac{j}{\omega(C_1+C_2)} \\ C_I = j\omega(C_1+C_2) \\ D_I = \frac{C_1+C_2}{C_3} + 1 \end{cases}$	$\begin{cases} A_{III} = \frac{C_5}{C_4} + 1 \\ B_{III} = j(\frac{\omega^2 C_5 L_3 L_4}{L_3+L_4} - 1)(\frac{C_4+C_5}{\omega C_4 C_5}) + \frac{j}{\omega C_5} \\ C_{III} = j\omega C_5 \\ D_{III} = -\frac{\omega^2 C_5 L_3 L_4}{L_3+L_4} + 1 \end{cases}$

The modified WPT system has the following advantages:

First, traditional WPT systems, such as SS compensated and parallel-parallel compensated WPT systems, only have a narrow impedance matching range. Therefore, some uncertain parameter changes cannot be compensated [32]. Compared with traditional WPT systems, the modified WPT system has more compensation components and a wider impedance matching range. To compensate the uncertain parameter changes, the impedance of the modified WPT system can be translated to any optimal impedance.

Second, the modified WPT system has two different operating modes. Each operating mode can be used to address a different variation range of the uncertain parameters. To obtain stable system efficiency, the modified WPT system can switch from one operating mode to the other mode using the single-pole double-throw switches.

Third, the parameters of the compensation components in the modified WPT system are optimally designed using an interval-based uncertain optimization method. Through this method, the WPT system can achieve good robustness performance to uncertain parameter variations. The system efficiency can remain nearly constant when the uncertain parameter (k, f, R_L or X_L) varies over a wide range. The details of the interval-based uncertain optimization method are given in the next section.

3.2. Interval-Based Uncertain Optimization Model

In this paper, an interval-based uncertain optimization method is proposed to enhance the robustness of the modified WPT system. Based on the method, an interval is used to model the uncertainty of a parameter (including coupling coefficient k, operating frequency f, load resistance R_L, and load reactance X_L). Thus, the WPT system can be analyzed and optimized based on the variation bounds of the uncertain parameters. There is no need to obtain the real-time information of the uncertain parameters.

Using the proposed method, the uncertainties of the parameters are described as:

$$U = \{M, R_L, X_L, f\},\ U \in I_U = [I_U^L, I_U^R] \tag{14}$$

where U represents the uncertain variable of the WPT system, I_U represents the variation interval of U, I_U^L, and I_U^R are the upper and lower bounds of I_U, respectively.

The modified WPT system has two operating modes. Each mode is used to address a different variation range of the uncertain variable. Therefore, I_U is divided into two subintervals.

$$I_{U1} = [I_U^L, I_U^D], \ I_{U2} = (I_U^D, I_U^R] \tag{15}$$

where, I_U^D is the division point, $I_U^D \in I_U$.

The parameters of the compensation components in the Q-type impedance matching networks can be written as:

$$X = \{L_1, L_2, L_3, L_4, C_1, C_2, C_3, C_4, C_5, C_6\}, \ X \in I_X = [I_X^L, I_X^R] \tag{16}$$

where X is the decision variable of the WPT system, I_X is the design space of X, I_X^L, and I_X^R are the upper and lower bounds of I_X, respectively.

By substituting the transmission parameters of the Q-type impedance matching networks (shown in Table 3) into Equation (13), the system efficiency of the modified WPT system can be obtained, which is the function of the uncertain variable U and the decision variable X.

$$\eta_S = F(X, U) \tag{17}$$

For any X, when the uncertain variable varies within the intervals I_{U1} and I_{U2}, the possible system efficiencies are two intervals:

$$\begin{cases} H_1 = [F_1^L(X), F_1^R(X)], \ U \in I_{U1} \\ H_2 = (F_2^L(X), F_2^R(X)], \ U \in I_{U2} \end{cases} \tag{18}$$

where $_i (i = 1, 2)$ is the variation interval of the system efficiency. $F_i^L(X)$ and $F_i^R(X)$ are the upper and the lower bounds of $_i$, which can be calculated using the following equations:

$$\begin{cases} F_i^L(X) = \min_U F(X, U) \\ F_i^R(X) = \max_U F(X, U) \\ U \in I_{Ui}, i = 1, 2 \end{cases} \tag{19}$$

To evaluate the performance of the modified WPT system, two objective functions are defined as follows:

$$\begin{cases} F^M(X, I_U^D) = -\left(\frac{F_1^L(X) + F_1^R(X) + F_2^L(X) + F_2^R(X)}{4} \right) \\ F^V(X, I_U^D) = \frac{\left(F_1^L(X) + F^M(X, I_U^D)\right)^2 + \left(F_1^R(X) + F^M(X, I_U^D)\right)^2}{4} \\ \quad + \frac{\left(F_2^L(X) + F^M(X, I_U^D)\right)^2 + \left(F_2^R(X) + F^M(X, I_U^D)\right)^2}{4} \end{cases} \tag{20}$$

$F^M(X, I_U^D)$ and $F^V(X, I_U^D)$ are the functions that depend on the decision variable X and the division point I_U^D. $F^M(X, I_U^D)$ is called the mean function of the system efficiency. It can be used to evaluate the average performance of the modified WPT system. The lower $F^M(X, I_U^D)$ is, the higher the average system efficiency is. $F^V(X, I_U^D)$ is called the variance function of the system efficiency. It can be used to evaluate the robustness performance of the modified WPT system. The lower $F^V(X, I_U^D)$ is, the less sensitive the system efficiency is to uncertain parameter variations.

For any two solutions, (X_1, I_U^{D1}) and (X_2, I_U^{D2}), if '$F^M(X_1, I_U^{D1}) < F^M(X_2, I_U^{D2})$' and '$F^V(X_1, I_U^{D1}) < F^V(X_2, I_U^{D2})$' are satisfied at the same time, it can be concluded that (X_1, I_U^{D1}) is better than (X_2, I_U^{D2}).

Finally, the interval-based uncertain optimization model for the WPT system can be obtained.

$$
\begin{cases}
\min_{X}\left(F^M(X, I_U^D), F^V(X, I_U^D)\right) \\
\text{Uncertain variable}: \ U \in I_{Ui}, \ (i = 1, 2) \\
\text{Decision variables}: \ X \in I_X, I_U^D \in I_U
\end{cases}
\tag{21}
$$

3.3. Bi-Level Nested Optimization Algorithm

Equation (21) is a bi-level nested optimization problem, in which the inner optimization is to find the variation bounds of the system efficiency when the uncertain parameters vary, and the outer optimization is to find the optimal solutions for the modified WPT system. However, because there is a nested optimization process, it is difficult to find the optimal solution using traditional gradient-based optimization algorithms. In this paper, the particle swarm optimization (PSO) algorithm [33] is used to solve the inner optimization problem, and the nondominated sorting genetic algorithm-II (NSGA-II) [34] is used to solve the outer optimization problem. The proposed optimization process is shown in Figure 5.

A numerical example of the modified WPT system is given in Table 4. Using the bi-level nested optimization algorithm, the optimal solutions for the modified WPT system can be obtained.
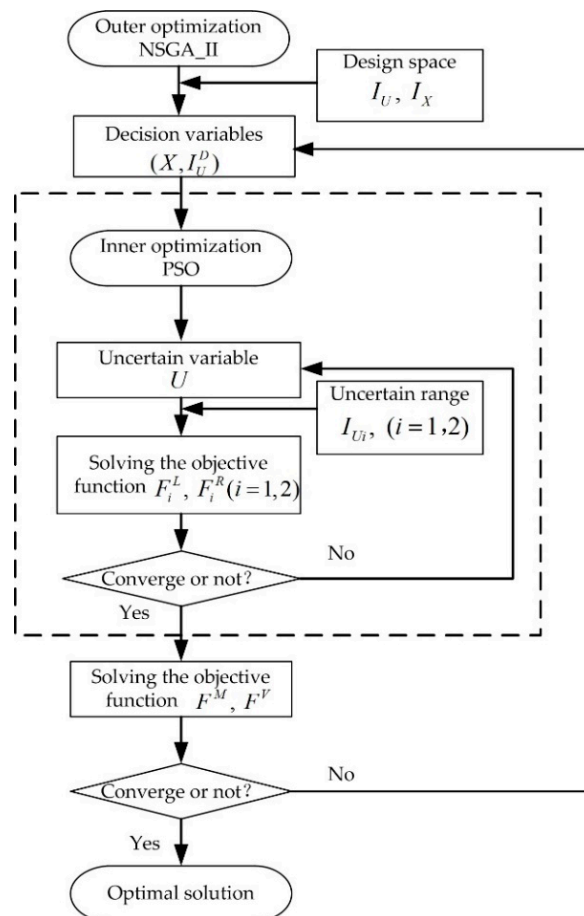

Figure 5. Bi-level nested optimization process.

Certain Parameter	Value
Source resistance R_S	50 Ω
Coil resistances R_T, R_R	1 Ω
Coil inductances L_T, L_R	30 μH
Uncertain Parameter	**Variation Interval**
Coupling coefficient k	[0.1, 0.6]
Operating frequency f	[1.5, 2.5] MHz
Load resistance R_L	[100, 1500] Ω
Load reactance X_L	[−800, 800] Ω

3.4. Optimization Results

Equation (21) is a double-objective optimization problem. In multi-objective optimization, because the objective functions are usually in conflict with each other, the optimal results are a group of Pareto optimal solutions. The Pareto front is the image of the Pareto optimal solutions viewed in objective space, which can offer valuable tradeoff information between objective functions [35,36].

3.4.1. Pareto Fronts

Figure 6 shows the Pareto fronts of the modified WPT system, from which it can be seen that the mean function $F^M(X, I_C)$ and the variance function $F^V(X, I_C)$ are in conflict with each other. The WPT system cannot achieve the highest average system efficiency and the best robustness performance at the same time. There is a need to make tradeoffs between them.
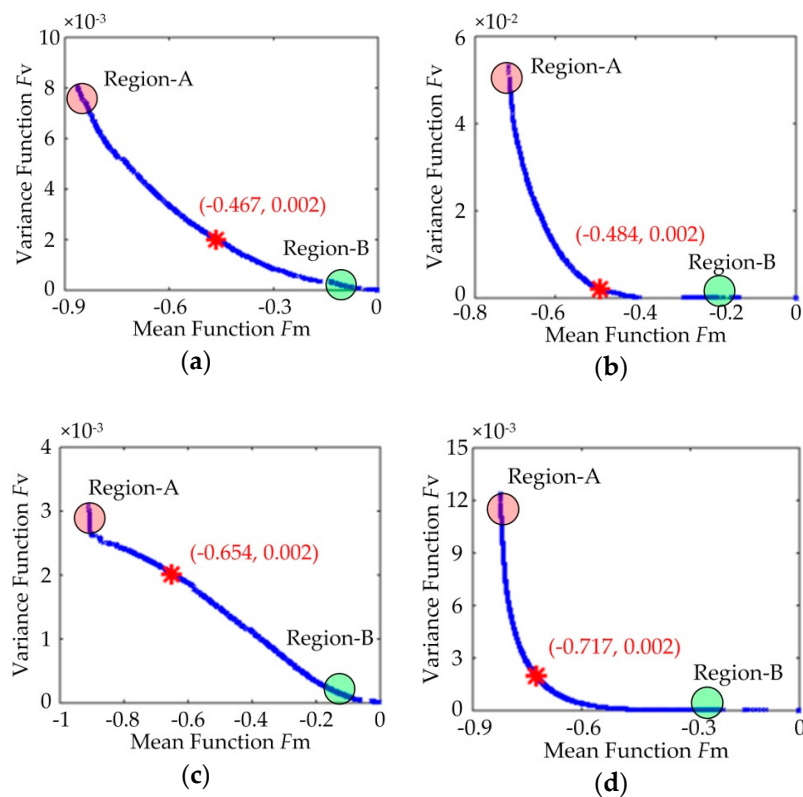

Figure 6. Pareto fronts of the optimal solutions: (**a**) the coupling coefficient k varies from 0.1 to 0.6; (**b**) the operating frequency f varies from 1.5 to 2.5 MHz; (**c**) the load resistance R_L varies from 100 to 1500 Ω; (**d**) the load reactance X_L varies from −800 to 800 Ω. (The initial values of the uncertain parameters are: $k = 0.2$, $f = 2$ MHz, $R_L = 300$ Ω, and $X_L = 0$ Ω).

The Pareto fronts can offer tradeoff information between the mean function and the variance function. As shown in Figure 6, the solutions within region-A have small mean function values and large variance function values. The modified WPT system will have high average system efficiency but poor robustness if these solutions are chosen. The solutions within region-B have large mean function values and small variance function values. The modified WPT system will have strong robustness but extremely low average system efficiency if these solutions are chosen. The solutions between region-A and region-B have medium average system efficiency and medium robustness. The decision should be made according to the practical application requirements.

3.4.2. Tradeoff Solutions

Because the goal of this paper is to enhance the robustness of the modified WPT system to uncertain parameter variations, the decision is made by: (1) $F^V(X, I_C) \leq 2 \times 10^{-3}$; (2) the lower $F^M(X, I_C)$ is, the better. Based on the rules, the tradeoff solutions can be found, which are marked with red asterisks in Figure 6.

Figure 7 shows the calculated system efficiencies (blue solid line) and matching factors (red dashed line) of the modified WPT system using the tradeoff solutions. It can be observed that the system efficiency of the modified WPT system only changes slightly when the coupling coefficient, the operating frequency, the load resistance or the load reactance varies over a wide range. It can be seen from Figure 7a–d that the average system efficiencies are 0.467, 0.484, 0.654, and 0.717, respectively. Therefore, the modified WPT system only achieves medium system efficiency.
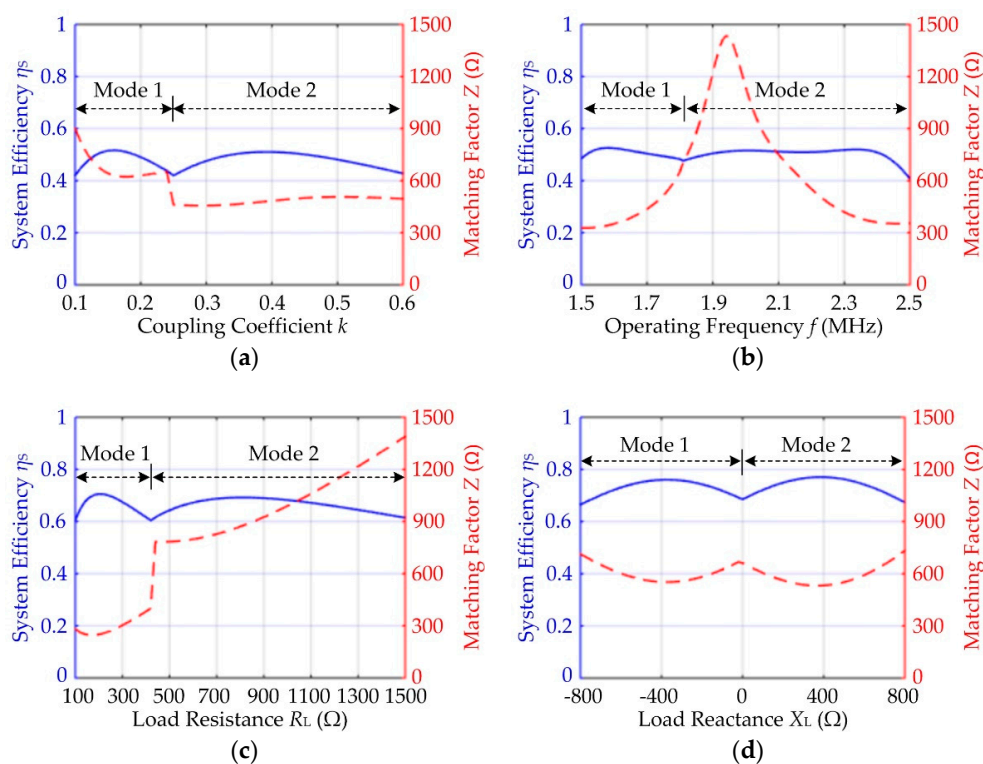

Figure 7. System efficiencies (blue solid line) and matching factors (red dashed line) of the modified WPT system: (**a**) the coupling coefficient k varies from 0.1 to 0.6; (**b**) the operating frequency f varies from 1.5 to 2.5 MHz; (**c**) the load resistance R_L varies from 100 to 1500 Ω; (**d**) the load reactance X_L varies from -800 to 800 Ω. (The initial values of the uncertain parameters are: $k = 0.2$, $f = 2$ MHz, $R_L = 300$ Ω, and $X_L = 0$ Ω.).

The matching factors can be used to evaluate the impedance matching status of the modified WPT system. In Figure 7a–d, it can be observed that the matching factor $Z \neq 0$ during the variations

of the coupling coefficient, the operating frequency, the load resistance, and the load reactance. Therefore, the modified WPT system using the tradeoff solutions does not achieve dual-side conjugated impedance matching.

Using the proposed method, the robustness of the modified WPT system to uncertain parameter variations can be significantly improved. However, the system efficiency does not reach the maximum value because the conjugated impedance matching condition '$Z = 0$' is not satisfied.

4. Experimental Verifications

In this section, a modified WPT system was implemented, and experimental studies were carried out to verify the theoretical method. For comparison, a SS compensated WPT system was also implemented and measured.

4.1. Hardware Implementations

4.1.1. Modified WPT System

The modified WPT system is shown in Figure 8. Two identical planar spiral coils, which were fabricated by Litz wires, were used as the power transmitter and receiver. The inner and outer diameters of the coils were 11 cm and 16.6 cm respectively. The number of turns of the coils was 10. An impedance analyzer was used to measure the electrical parameters of the coils. The measured inductance and resistance of the transmitter coil were 24.1 µH and 3.2 Ω, respectively. The measured inductance and resistance of the receiver coil were 21.8 µH and 4.5 Ω, respectively. For the convenience of implementation, the transmitter coil and the receiver coil were placed coaxially, and the longitudinal distance between the coils was adjusted to implement the coupling coefficient variation. The coupling coefficient could be varied from 0.15 to 0.55 by adjusting the longitudinal distance between the coils. This operation can be used to simulate other coil displacements which lead to the same coupling coefficient variation.

A power amplifier was used to input power to the transmitter coil. The operating frequency of the power amplifier could be adjusted from 1.5 to 2.5 MHz (Such a frequency range was chosen because the power processing circuits with this operating frequency range is commercially available and easy to implement [26]). The output resistance of the power amplifier was 50 Ω. A load was used to consume the power received by the receiver coil. The load resistance could be adjusted from 50 Ω to 1050 Ω, and the load reactance could be adjusted from −300 Ω to 300 Ω.
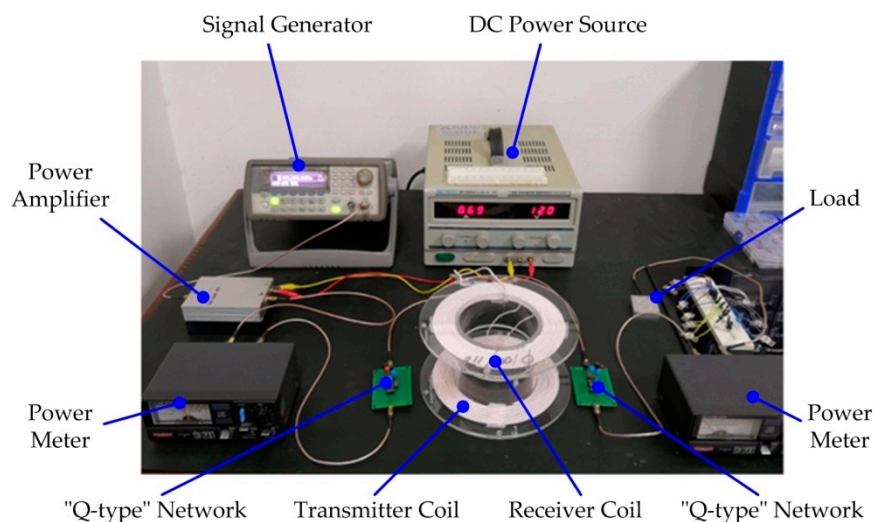

Figure 8. The modified WPT system.

In the modified WPT system, one Q-type impedance matching network was connected between the power amplifier and the transmitter coil, and the other Q-type impedance matching network was connected between the load and the receiver coil. The parameters of the compensation components in the Q-type impedance matching networks were optimally designed using the proposed interval-based uncertain optimization method. The tradeoff solutions obtained are shown in Table 5.

Table 5. The tradeoff solutions for the modified WPT system.

Item		Uncertain Variables			
		k **Varies in** **[0.15, 0.55]**	f **Varies in** **[1.5, 2.5] MHz**	R_L **Varies in** **[50, 1050] Ω**	X_L **Varies in** **[−300, 300] Ω**
Tradeoff solutions	I_U^D	0.25	1.8 MHz	250 Ω	0 Ω
	$L_1(\mu H)$	23.4	5.9	5.6	7.3
	$L_2(\mu H)$	500.0	87.5	177.4	481.5
	$L_3(\mu H)$	16.5	5.0	17.5	31.8
	$L_4(\mu H)$	473.3	245.4	98.0	435.1
	$C_1(pF)$	50.1	173.6	52.8	508.1
	$C_2(pF)$	576.7	770.2	740.0	130.1
	$C_3(pF)$	936.2	367.7	422.2	219.6
	$C_4(pF)$	1079.8	442.6	471.1	666.4
	$C_5(pF)$	491.7	988.7	850.0	625.5
	$C_6(pF)$	230.4	60.4	285.6	70.3
Objective functions	F^M	0.735	0.463	0.727	0.412
	F^V	0.002	0.002	0.002	0.002

4.1.2. SS Compensated WPT System

For comparison purposes, a SS compensated WPT system (which is one of the most commonly used structures [29–31]) was also implemented. As shown in Figure 9, the power source, the transmitter coil, the receiver coil, and the load in the SS compensated WPT system were the same with those in the modified WPT system shown in Figure 8.

The difference is that the SS compensated WPT system only includes two compensation capacitors (C_T, C_R). In the experimental study, the resonance frequency of the SS compensated WPT system was adjusted to 2 MHz by setting $C_T = 265.3$ pF and $C_R = 278.7$ pF.
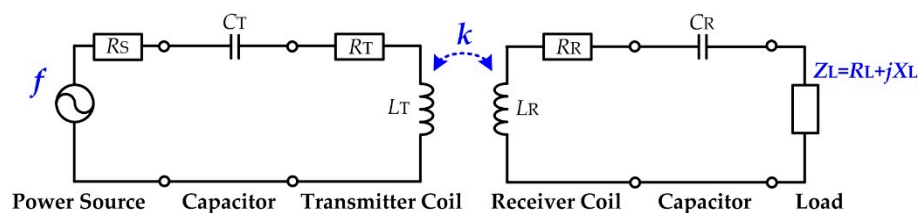

Figure 9. The SS compensated WPT system.

4.2. Experimental Results

Based on Equation (13), the system efficiencies of the two kinds of WPT systems can be calculated theoretically. In the experimental study, two power meters (as shown in Figure 8) were used to measure the source output power and the load power, respectively. Then, the actual system efficiencies of the two kinds of WPT systems can be obtained.

When the coupling coefficient k, the operating frequency f, the load resistance R_L or the load reactance X_L varies, the system efficiencies of the two kinds of WPT systems are shown in Figure 10a–d, respectively. The purple dashed lines (S1-Cal.) and blue solid lines (S1-Exp.) represent the calculated and measured system efficiencies of the modified WPT system respectively. The green dotted lines

(S2-Cal.) and red solid lines (S2-Exp.) represent the calculated and measured system efficiencies of the SS compensated WPT system respectively.

It can be observed that the calculated system efficiency curves and the measured system efficiency curves have the same variation trends. However, at some points, the measured values are much lower than the calculated ones. The possible reasons include: (1) The errors between the theoretical and actual capacitance/inductance of the compensation components lead to the decrease of the system efficiency; (2) In theoretical calculations, the compensation capacitors/inductors are assumed to be ideal energy-storage components without any energy losses. But in the experimental study, these compensation components will consume a small part of the total power in the forms of heat and result in the decrease of the system efficiency.
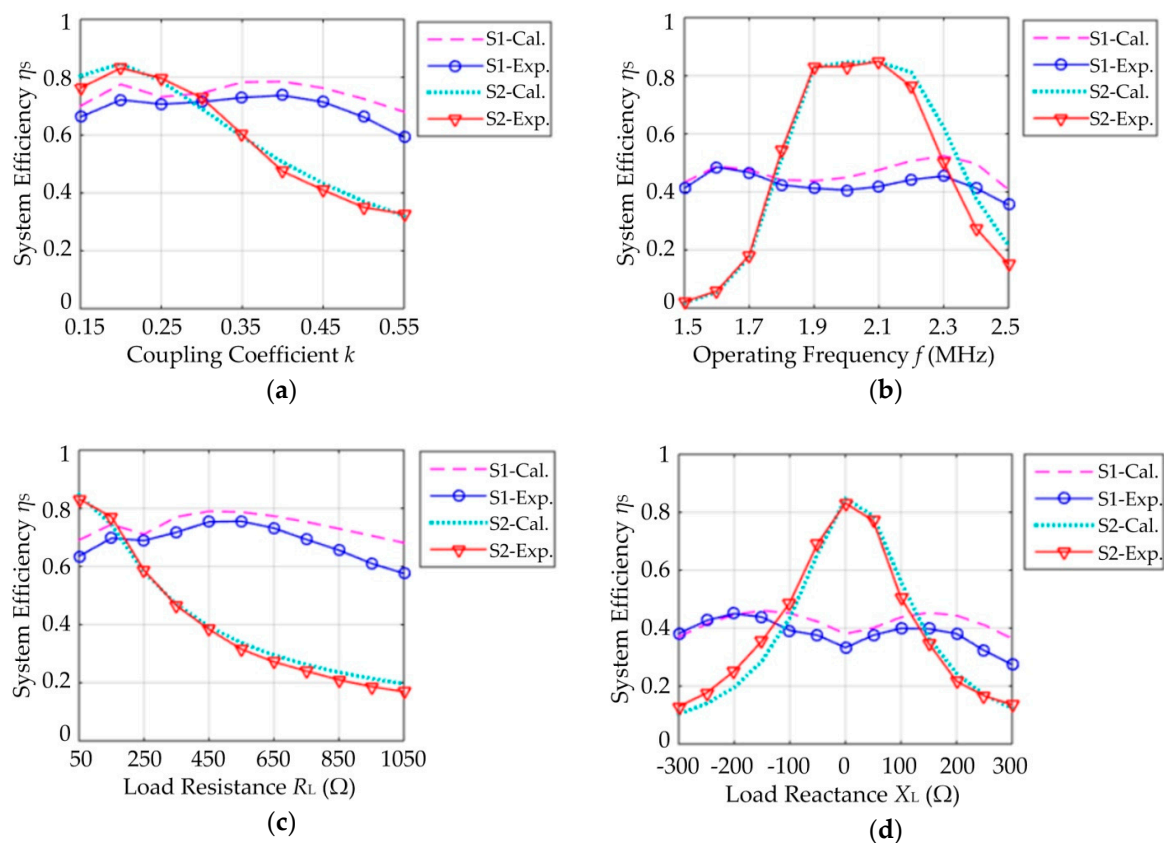

Figure 10. System efficiencies of two kinds of WPT systems: (**a**) the coupling coefficient *k* varies from 0.15 to 0.55; (**b**) the operating frequency *f* varies from 1.5 to 2.5 MHz; (**c**) the load resistance R_L varies from 50 to 1050 Ω; (**d**) the load reactance X_L varies from −300 to 300 Ω. (The initial values of the uncertain parameters are: *k* = 0.2, *f* = 2 MHz, R_L = 50 Ω, and X_L = 0 Ω).

It can be observed from Figure 10a–d that the measured maximum system efficiency of the SS compensated WPT system are 0.832, 0.850, 0.832, and 0.832 respectively, and the measured minimum system efficiency of the SS compensated WPT system are 0.328, 0.021, 0.170, and 0.129 respectively. The measurement results show that the system efficiency of the SS compensated WPT system is very sensitive to the variation of the coupling coefficient, the operating frequency, the load resistance or the load reactance.

It can be observed from Figure 10a–d that the measured maximum system efficiency of the modified WPT system are 0.737, 0.486, 0.755, and 0.450 respectively, and the measured minimum system efficiency of the modified WPT system are 0.592, 0.355, 0.576, and 0.274 respectively. The measurement results show that the system efficiency of the modified WPT system only changes slightly when the

coupling coefficient, the operating frequency, the load resistance or the load reactance varies over a wide range.

The experimental results demonstrate that the modified WPT system has better robustness than the SS compensated WPT system. The SS compensated WPT system can achieve the maximum system efficiency at some points. Compared with the SS compensated WPT system, the modified WPT system can only achieve medium system efficiency.

5. Conclusions

In this paper, a modified WPT system structure and an interval-based uncertain optimization method are proposed to enhance the robustness of the WPT system to uncertain parameter variations. To verify the effectiveness of the proposed method, two kinds of WPT systems were implemented and measured. The main results of this paper can be summarized as follows:

1. A modified WPT system structure is proposed in this paper. Two Q-type impedance matching networks are inserted in the transmitter circuit and the receiver circuit, respectively. By doing so, the modified WPT system can operate at two different modes. To address uncertain parameter variations, the modified WPT system can switch from one operating mode to the other mode, which is efficient and easy to implement.
2. An interval-based uncertain optimization method is proposed to enhance the robustness of the modified WPT system. A double-objective uncertain optimization model for the modified WPT system is built, and a bi-level nested optimization algorithm is proposed to find robust solutions. Through this method, the modified WPT system can achieve good robustness performance when the coupling coefficient, the operating frequency, the load resistance or the load reactance varies over a wide range.
3. Compared with active control methods, the proposed method in this paper only uses passive compensation networks (Q-type impedance matching networks). Therefore, the structure and control difficulty of the WPT system can be reduced. The size of the Q-type networks can be made small, which contributes to the miniaturization of the overall system. The proposed method is more suitable for some applications where high robustness performance, medium system efficiency, and a small system size are required.

Author Contributions: Y.Y. conceived this study. Y.L. designed the methodology and performed the experiments. M.C. carried out the data analysis. X.W. provided guidance for this study. All authors contributed to the writing of this paper.

Conflicts of Interest: The authors declare no conflict of interest.

References

1. Hwang, I.; Jang, Y.J.; Ko, Y.D.; Lee, M.S. System optimization for dynamic wireless charging electric vehicles operating in a multiple-route environment. *IEEE Trans. Intell. Transp. Syst.* **2017**, *99*, 1–18. [CrossRef]
2. Assawaworrarit, S.; Yu, X.; Fan, S. Robust wireless power transfer using a nonlinear parity-time-symmetric circuit. *Nature* **2017**, *546*, 387–390. [CrossRef] [PubMed]
3. Patil, D.; Mcdonough, M.; Miller, J.; Fahimi, B.; Balsara, P.T. Wireless power transfer for vehicular applications: Overview and challenges. *IEEE Trans. Transp. Electrification* **2018**, *4*, 3–37. [CrossRef]
4. Diekhans, T.; De Doncker, R.W. A dual-side controlled inductive power transfer system optimized for large coupling factor variations and partial load. *IEEE Trans. Power Electron.* **2015**, *30*, 6320–6328. [CrossRef]
5. Hwang, K.; Cho, J.; Kim, D.; Park, J.; Kwon, J.H.; Kwak, S.I.; Park, H.H.; Ahn, S. An autonomous coil alignment system for the dynamic wireless charging of electric vehicles to minimize lateral misalignment. *Energies* **2017**, *10*, 315. [CrossRef]
6. Orekan, T.; Zhang, P.; Shih, C. Analysis, design, and maximum power-efficiency tracking for undersea wireless power transfer. *IEEE J. Emerg. Sel. Top. Power Electron.* **2018**, *6*, 843–854. [CrossRef]

7. Huang, S.; Li, Z.; Lu, K. Transfer efficiency analysis of wireless power transfer system under frequency drift. *J. Appl. Phys.* **2015**, *117*, 17E706. [CrossRef]

8. Chabalko, M.; Besnoff, J.; Laifenfeld, M.; Ricketts, D.S. Resonantly coupled wireless power transfer for non-stationary loads with application in automotive environments. *IEEE Trans. Ind. Electron.* **2017**, *64*, 91–103. [CrossRef]

9. Fu, M.; Yin, H.; Zhu, X.; Ma, C. Analysis and tracking of optimal load in wireless power transfer systems. *IEEE Trans. Power Electron.* **2015**, *30*, 3952–3963. [CrossRef]

10. Mercier, P.P.; Chandrakasan, A.P. Rapid wireless capacitor charging using a multi-tapped inductively coupled secondary coil. *IEEE Trans. Circuits Syst.* **2013**, *60*, 2263–2272. [CrossRef]

11. Xiao, C.; Liu, Y.; Cheng, D.; Wei, K. New insight of maximum transferred power by matching capacitance of a wireless power transfer system. *Energies* **2017**, *10*, 688. [CrossRef]

12. Heebl, J.D.; Thomas, E.M.; Penno, R.P.; Grbic, A. Comprehensive analysis and measurement of frequency-tuned and impedance-tuned wireless non-radiative power-transfer systems. *IEEE Antennas Propag. Mag.* **2014**, *56*, 44–60. [CrossRef]

13. Kim, N.Y.; Kim, K.Y.; Choi, J.; Kim, C.W. Adaptive frequency with power-level tracking system for efficient magnetic resonance wireless power transfer. *Electron. Lett.* **2012**, *48*, 452–454. [CrossRef]

14. Huang, S.; Li, Z.; Lu, K. Frequency splitting suppression method for four-coil wireless power transfer system. *IET Power Electron.* **2016**, *9*, 2859–2864. [CrossRef]

15. Beh, T.C.; Kato, M.; Imura, T.; Oh, S.; Hori, Y. Automated impedance matching system for robust wireless power transfer via magnetic resonance coupling. *IEEE Trans. Ind. Electron.* **2013**, *60*, 3689–3698. [CrossRef]

16. Luo, Y.; Yang, Y.; Chen, Z. Self-tuning wireless power transmission scheme based on on-line scattering parameters measurement and two-side power matching. *Sci. Rep.* **2014**, *4*, 4332. [CrossRef] [PubMed]

17. Zou, Y.; Dai, X.; Li, W.; Sun, Y. Robust design optimisation for inductive power transfer systems from topology collection based on an evolutionary multi-objective algorithm. *IET Power Electron.* **2015**, *8*, 1767–1776. [CrossRef]

18. Ahn, D.; Kim, S.; Moon, J.; Cho, I.K. Wireless power transfer with automatic feedback control of load resistance transformation. *IEEE Trans. Power Electron.* **2016**, *31*, 7876–7886. [CrossRef]

19. Li, Y.; Duan, Q.; Zou, Y. High robustness control for robotic wireless power transfer systems with multiple uncertain parameters using a virtual buck converter. *Energies* **2017**, *10*, 517. [CrossRef]

20. Rentschler, M.; Bhattacharya, I. Decoupled control of wireless power transfer: Eliminating the interdependence of load resistance and coupling to achieve a simple control framework with fast response times. *Int. J. Electr. Power Energy Syst.* **2018**, *99*, 156–163. [CrossRef]

21. Su, Y.G.; Zhang, H.Y.; Wang, Z.H.; Hu, A.P.; Chen, L.; Sun, Y. Steady-state load identification method of inductive power transfer system based on switching capacitors. *IEEE Trans. Power Electron.* **2015**, *30*, 6349–6355. [CrossRef]

22. Dai, X.; Li, X.; Li, Y.; Deng, P.; Tang, C. A maximum power transfer tracking method for WPT systems with coupling coefficient identification considering two-value problem. *Energies* **2017**, *10*, 1665. [CrossRef]

23. Dai, X.; Li, X.; Li, Y.; Hu, A.P. Maximum efficiency tracking for wireless power transfer systems with dynamic coupling coefficient estimation. *IEEE Trans. Power Electron.* **2018**, *33*, 5005–5015. [CrossRef]

24. Lim, Y.; Tang, H.; Lim, S.; Park, J. An adaptive impedance-matching network based on a novel capacitor matrix for wireless power transfer. *IEEE Trans. Power Electron.* **2014**, *29*, 4403–4413. [CrossRef]

25. Li, S.; Li, W.; Deng, J.; Nguyen, T.D.; Mi, C.C. A double-sided LCC compensation network and its tuning method for wireless power transfer. *IEEE Trans. Veh. Technol.* **2015**, *64*, 2261–2273. [CrossRef]

26. Hui, S.Y.R.; Zhong, W.; Lee, C.K. A critical review of recent progress in mid-range wireless power transfer. *IEEE Trans. Power Electron.* **2014**, *29*, 4500–4511. [CrossRef]

27. Luo, Y.; Yang, Y.; Chen, S.; Wen, X. A frequency-tracking and impedance-matching combined system for robust wireless power transfer. *Int. J. Antenn. Propag.* **2017**, *2017*, 1–13. [CrossRef]

28. Ye, W.; Chen, L.; Liu, F.; Chen, X.; Wang, X. Analysis and optimization of 3-coil magnetically coupled resonant wireless power transfer system for stable power transmission. In Proceedings of the IEEE Energy Conversion Congress and Exposition (ECCE), Cincinnati, OH, USA, 1–5 October 2017; pp. 2584–2589.

29. Feng, H.; Cai, T.; Duan, S.; Zhang, X.; Hu, H.; Niu, J. A Dual-side-detuned series–series compensated resonant converter for wide charging region in a wireless power transfer system. *IEEE Trans. Ind. Electron.* **2018**, *65*, 2177–2188. [CrossRef]

30. Zhang, W.; Wong, S.C.; Chi, K.T.; Chen, Q. Design for efficiency optimization and voltage controllability of series–series compensated inductive power transfer systems. *IEEE Trans. Power Electron.* **2014**, *29*, 191–200. [CrossRef]

31. Yang, Y.; Zhong, W.; Kiratipongvoot, S.; Tan, S.C.; Hui, S.Y.R. Dynamic improvement of series–series compensated wireless power transfer systems using discrete sliding mode control. *IEEE Trans. Power Electron.* **2018**, *33*, 6351–6360. [CrossRef]

32. Liu, S.; Liu, M.; Yang, S.; Ma, C.; Zhu, X. A novel design methodology for high-efficiency current-mode and voltage-mode class-E power amplifiers in wireless power transfer systems. *IEEE Trans. Power Electron.* **2017**, *32*, 4514–4523. [CrossRef]

33. Shi, Y. Particle swarm optimization: Developments, applications and resources. In evolutionary computation. In Proceedings of the 2001 Congress on Evolutionary Computation, Seoul, Korea, 27–30 May 2001; pp. 81–86.

34. Deb, K.; Pratap, A.; Agarwal, S.; Meyarivan, T.A.M.T. A fast and elitist multiobjective genetic algorithm: NSGA-II. *IEEE Trans. Evol. Comput.* **2002**, *6*, 182–197. [CrossRef]

35. Pereyra, V.; Saunders, M.; Castillo, J. Equispaced Pareto front construction for constrained bi-objective optimization. *Math. Comput. Model.* **2013**, *57*, 2122–2131. [CrossRef]

36. Cai, Z.; Wang, Y. A multiobjective optimization-based evolutionary algorithm for constrained optimization. *IEEE Trans. Evol. Comput.* **2006**, *10*, 658–675. [CrossRef]